Chapter 15

Simple Method for Constructing RNA Triangle, Square, Pentagon by Tuning Interior RNA 3WJ Angle from 60° to 90° or 108°

Emil F. Khisamutdinov, My Nguyen Hoan Bui, Daniel Jasinski, Zhengyi Zhao, Zheng Cui, and Peixuan Guo

Abstract

Precise shape control of architectures at the nanometer scale is an intriguing but extremely challenging facet. RNA has recently emerged as a unique material and thermostable building block for use in nanoparticle construction. Here, we describe a simple method from design to synthesis of RNA triangle, square, and pentagon by stretching RNA 3WJ native angle from 60° to 90° and 108°, using the three-way junction (3WJ) of the pRNA from bacteriophage phi29 dsDNA packaging motor. These methods for the construction of elegant polygons can be applied to other RNA building blocks including the utilization and application of RNA 4-way, 5-way, and other multi-way junctions.

Key words RNA nanotechnology, RNA nanoparticles, *In silico* design, pRNA 3WJ

1 Introduction

RNA nanotechnology has seen rapid growth as a new platform since 1998 when the concept was first introduced [1]. The ability to manipulate RNA molecules to fabricate nanometer-scale particles with predictable geometrical and functional properties has resulted in a renewed interest in nanosized material construction and nanotechnology including optical sensing [2–4], delivery of therapeutics [5–12], computer design [13, 14], and intracellular detection imaging [15, 16]. Nucleic acids, both DNA and RNA, represent natural polymers and, despite having similar monomeric composition (ATCG in DNA and AUCG in RNA), are very different in folding and biological function. While DNA's primary role is to carry genetic information and the molecule mainly exists as a right-handed double B-form helix, RNA is much more versatile, as this biopolymer can fold into a variety of secondary and tertiary structures allowing it to perform multiple functions in nature

Luc Ponchon (ed.), *RNA Scaffolds: Methods and Protocols*, Methods in Molecular Biology, vol. 1316,
DOI 10.1007/978-1-4939-2730-2_15,

including gene transfer functions (mRNA) [17], adaptor functions (tRNAs) [18–20], guide functions (snRNAs, snoRNAs) [21–23], catalytic functions (ribozymes and the large ribosomal RNA) [24–26], and environmental sensing functions (riboswitches) [27, 28]. It rarely exists just in double-stranded form, which is A-form configuration. Base-stacking and noncanonical base-paring in RNA provide more room for the design of RNA nanoarchitectures [29].

RNA tertiary structures display a degree of flexibility, which is beneficial for nanofabrication of diverse particles. RNA's flexibility has been well documented by the structural analysis of natural RNA nanomachines such as ribosomes where whole subunits undergo ratchet motions during protein synthesis [30–32], and some individual junctions and internal loops can bend from 180° to 60°, e.g., kink-turn motif [33, 34]. Riboswitches are other natural RNA devices that possess flexibility; upon binding a specific ligand, conformational change occurs that signals for induction or reduction of protein synthesis [27].

Phi29 packaging RNA, or pRNA, forms a hexameric ring that gears the packaging of DNA into a preformed protein capsid [35–37]. An unusually stable three-way junction (3WJ) motif has recently been found within this pRNA molecule [11, 38]. This structural module of the pRNA has attracted scientific attention not only because of its applications to deliver therapeutic moieties to target cells due to its thermostable properly, but also as a building block for fabricating stable nanoparticles of different sizes and shapes [39–41]. Detailed analysis of the crystal structure of phi29 pRNA 3WJ motif demonstrated that it is composed of not only Watson–Crick base pairs, but also noncanonical interactions; these include a cis Watson–Crick Watson–Crick (cWW) U-U pair, a base-phosphate (BPh) G-U pair, and two wobble G-U pairs. Additionally, crystal structure analysis revealed that the 3WJ motif was uniquely coordinated by two Mg^{2+} ions that allow stable conformational changes. The 3WJ geometry is a typical A-type [42] and contains three helices: H1, H2, and H3. H1 and H3 form coaxial stacking, aligning along a common axis, and forming ~180° angle. The overall orientation of the motif is planar and helices H1 and H2 form a 60° angle that has been observed in the A-type 3WJs (Fig. 1a). Based on thermodynamic properties and flexibility of the pRNA 3WJ module, we describe a simple method for the construction of various RNA polygons including triangle, square, and pentagon by stretching one of the three 3WJ angles from 60° to 90° and to 108°.

2 Materials

1. PCR reaction kit: Several kits are commercially available; however we use the kit from Promega Corporation, GoTaq® FlexiDNA Polymerase.

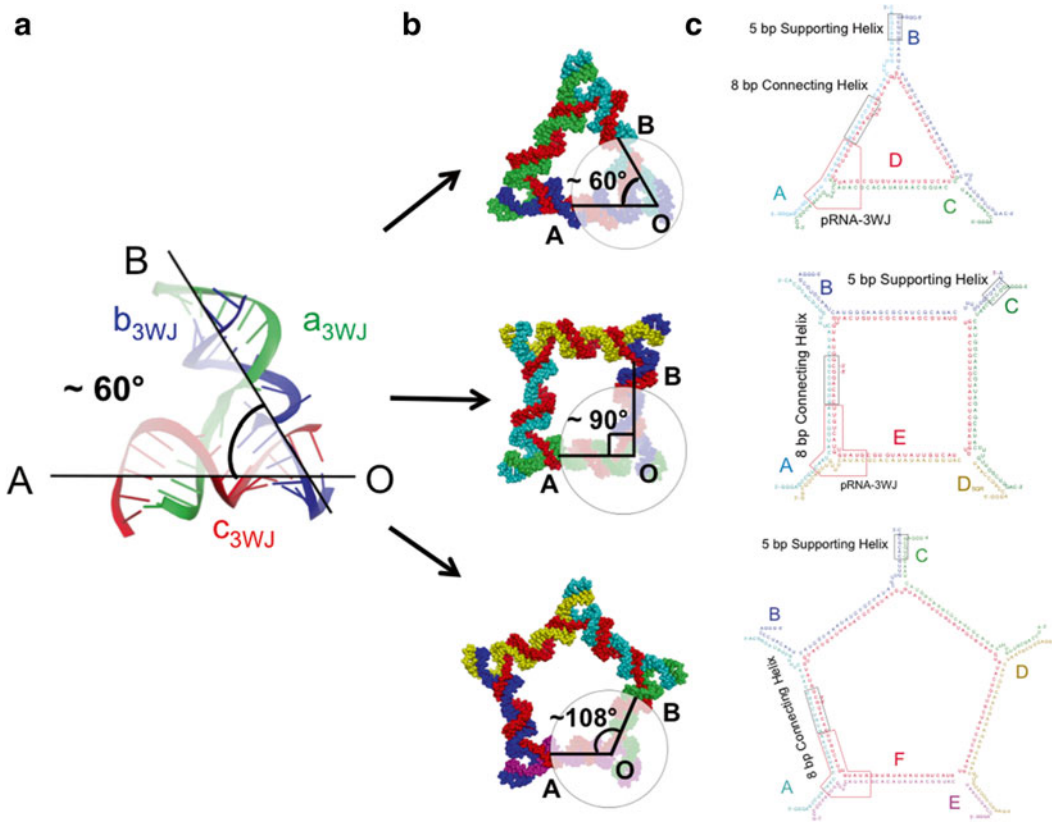

Fig. 1 Structure of pRNA 3WJ and RNA polygons. (**a**) Crystal structure of pRNA-3WJ showing internal ∠AOB angle used to construct polygons. (**b**) 3D models of RNA polygons with internal angles highlighted with a *circle*. (**c**) Sequences and 2D structures of RNA polygons showing connecting helices and supporting helices

2. DNA primers for in vitro RNA transcription dissolved in double-deionized water (dd H_2O) 100 μM stock concentration.
3. QIAquick PCR Purification Kit (http://www.qiagen.com/, cat #28706).
4. Ethylenediaminetetraacetic acid (EDTA) 0.5 M, pH = 8.0.
5. Tris-acetate-EDTA (TAE) buffer, pH = 8.0; 1× buffer composition: 40 mM Tris base, 20 mM acetic acid, and 1 mM EDTA.
6. Tris-borate EDTA (TBE) buffer, pH = 8.0; 1× buffer composition: 89 mM Tris base, 86 mM boric acid, and 2 mM EDTA.
7. Tris-borate-magnesium (TBM) buffer, pH = 8.0; 1× buffer composition: 89 mM Tris base, 86 mM boric acid, and 5 mM $MgCl_2$.
8. Sodium acetate 3 M, pH = 6.5.
9. Tris-magnesium saline buffer, pH = 8.0; 1× buffer composition: 50 mM Tris–HCl, 100 mM NaCl, 10 mM $MgCl_2$.

10. Urea 8 M in 20 mM TBE buffer pH = 8.0.
11. RNA elution buffer: 0.5 M NH_4OAc, 10 mM EDTA, 0.1 % SDS.
12. Denaturing polyacrylamide; stock 20 % solution composition: Acrylamide/*bis*-acrylamide (29:1), 8 M urea, 1× TBE buffer.
13. RNA nucleotide triphosphates (rNTP) 100 mM, adjust pH to 7.5 with NaOH.
14. Fluorine-modified UTP and CTP at 2′ hydroxyl ribose (2′F-UTP and 2′F-CTP).
15. T7 RNA polymerase transcription buffer; 1× buffer composition: 40 mM HEPES-KOH pH = 7.5, 24 mM $MgCl_2$, 2 mM spermidine, 2 mM, 40 mM DTT.
16. 2′F-transcription buffer; 1× buffer composition: 40 mM Tris-acetate pH = 8.0, 0.5 mM DTT, 1 mM EDTA, 10 mM $Mg(OAc)_2$, 0.5 mM $MnCl_2$, 16 mM spermidine.
17. 3 M Sodium acetate solution in ddH_2O.
18. Temperature gradient gel electrophoresis (TGGE) Standard system, Biometra.
19. PAGE Gel Imaging System: Typhoon FLA 7000.

3 Methods

Detailed procedures describing RNA synthesis, purification, self-assembly, and analysis have been detailed previously [10]. Below, we briefly describe some steps of RNA nanoparticle fabrication and comparison of their thermal stabilities. Synthetic DNA molecules coding for the antisense sequence of the desired RNA were purchased from IDT DNA (www.idtdna.com) and amplified by Polymerase Chain Reaction (Promega Corporation) using primers containing the T7 RNA polymerase promoter sequence (5′-TA ATACGACTCACTATA-3′).

3.1 DNA Amplification via PCR Reaction

1. Follow the recommended protocol from Promega Co, summarized below.

Protocol 1. PCR reaction setup	
57 µL	ddH_2O
20 µL	5× GoTaq Buffer
10 µL	25 mM $MgCl_2$
8 µL	2.5 mM dNTPs
2 µL	100 µM FRW primer[a]
2 µL	100 µM REV primer[b]

(continued)

(continued)

1 μL	Go Taq polymerase
V_{total} = 100 μL	

[a]FRW—forward DNA primer containing T7 RNA polymerase promoter sequence
[b]REV—reverse DNA primer

On a thermal cycler set up the following steps:

Step #1: 95 °C for 5 min.

Step #2: 95 °C for 1 min.

Step #3: 55 °C for 1 min.

Step #4: 72 °C for 1 min.

Step #5: Repeat Steps #2, 3, and 4 25 times.

Step #6: 72 °C for 5 min.

Step #7: 4 °C for 12 h.

2. Purify PCR products using QIAquick PCR Purification Kit; follow the manufacturer's protocol for purification steps. Usually, DNA concentration is 0.1–0.2 μg/μL after purification.
3. Check approximate length of purified DNA templates on 2 % agarose gel using 1× TAE buffer prior to RNA transcription reaction, *see* **Note 1**.

3.2 RNA and 2′ F-U/C RNA Enzymatic Synthesis

1. Reaction mixtures should be prepared at room temperature. There are two protocols given below that have been applied to template DNAs directing transcription from the T7 class III promoter. Protocol #2 summarizes reagent composition for regular RNA transcription reaction. To produce nuclease-resistant 2′-fluoro-modified RNAs we utilize Y639F mutant T7 RNAP and replace pyrimidines (rUTP and rCTP) with the corresponding 2′-fluoro-analogs (http://www.trilinkbiotech.com/); please refer to protocol #3 below.

Protocol 2. In vitro RNA transcription by T7 RNA polymerase	
5 μL	ddH_2O
10 μL	5× Transcription buffer
10 μL	25 mM rNTPs
5 μL	100 mM DTT
10 μL	DNA template
10 μL	T7 RNA polymerase
V_{total} = 50 μL	

Incubate the mixture at 37 °C for 4–6 h.
Transcription can be scaled up using the same ratios.

Protocol 3. In vitro 2′F-U/C-modified RNA transcription by Y639F RNA polymerase	
5 μL	ddH_2O
5 μL	10× 2′F-transcription buffer
5 μL	100 mM DTT
5 μL	50 mM 2′-F CTP
5 μL	50 mM 2′-F UTP
5 μL	50 mM rGTP
5 μL	50 mM rATP
10 μL	DNA template
5 μL	Y639F RNA polymerase
$V_{total} = 50$ μL	

Incubate the mixture at 37 °C overnight.
Transcription can be scaled up using the same ratios.

2. Terminate transcription reaction by adding 1 μL of RNase-free DNase I and incubate for additional 30 min to hydrolyze DNA primers.
3. Add the same amount of 8 M urea in TBE to the transcription reaction and run the samples on denaturing PAGE (15 % acrylamide, 29:1 acrylamide:bis-acrylamide, 8 M urea) in 1× TBE buffer at 120 V at ambient temperature.
4. Place the gel on a TLC plate and excise the RNA band under UV light. Extract RNA from gel slices using 0.5 mL of RNA elution with 2-h incubation at 37 °C.
5. Precipitate RNA molecules with cold ethanol (2.5:1 (Ethanol:RNA) volume ratio) and 3 M sodium acetate (1:10 volume ratio), rinse twice with cold 80 % ethanol, dry under vacuum, and redissolve in dd H_2O.
6. Measure RNA concentration and store all samples at −20 °C and also, refer to the **Notes 2** and **3** for troubleshoot.

3.3 Stretching the Intra-helical Angle Formed Between H1 and H2

Three-dimensional computer models of the RNA triangle, square, and pentagons were built by manual alignment and adjustments of the pRNA 3WJ junction using Swiss-PDB viewer. For example, the triangle model was constructed by aligning 3× 3WJ motifs at the correct angle and distance by "auto-fit" tool or by manual adjustment in Swiss-PDB viewer. H1 was then connected to H2 of each adjacent 3WJ module by double-stranded A-type RNA helix. This "connecting" helix is eight base pairs in length, which results in flat nanoparticles, detailed structure being illustrated in Fig. 1. At each corner, the external helix of the 3WJ is extended by five base pairs as a "supporting" helix to increase stability and specificity among strands. The resulting models contained the 3WJ motif at the

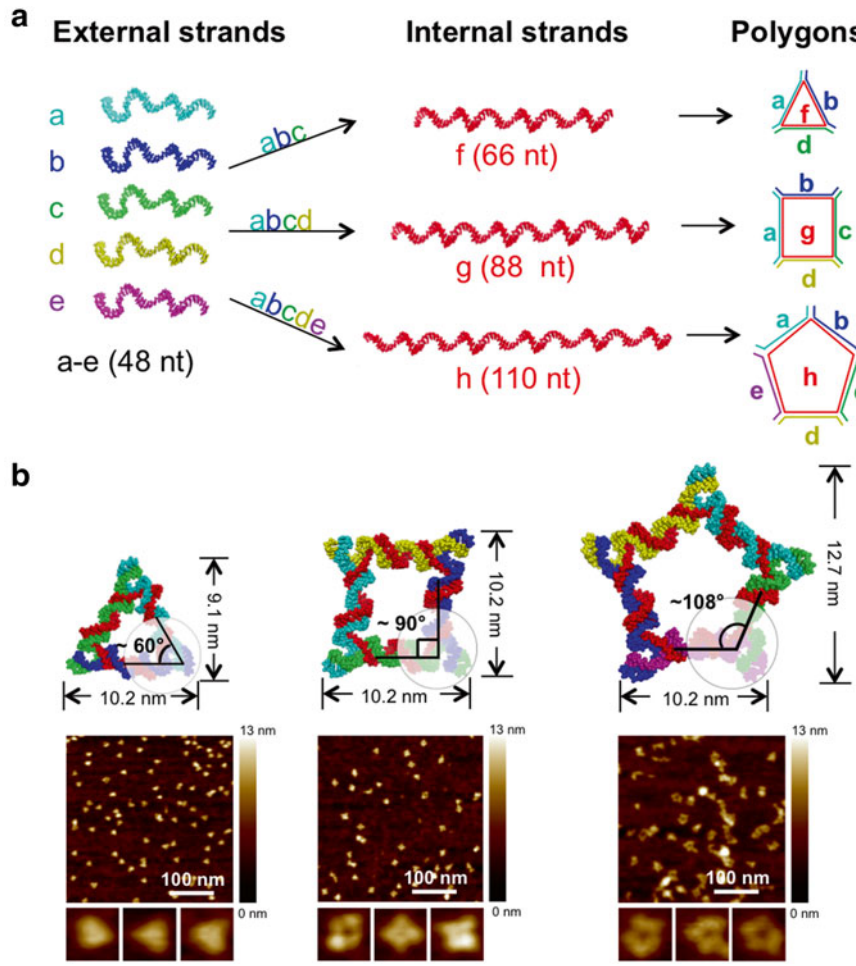

Fig. 2 Construction method of RNA polygons. (**a**) Combination of external strands with specific internal strand results in corresponding polygons. (**b**) Annotated size models of RNA polygons and corresponding AFM images are *below* the models

corners with the inner angle of each polygon corresponding to ∠AOB (Fig. 1b). The 3D models are composed of different numbers of RNA strands called short strands (external) and long strands (internal) as shown in Fig. 2a. The number of short strands corresponds to the number of sides of the corresponding polygon, with the internal strand interconnecting all external strands, generating compact structures that are completely double stranded. For example, construction of the triangular nanoparticle consists of three short external RNA strands and one long internal strand, resulting in a 3:1 ratio of short strands to long strands. To build the square nanoparticle this ratio should be 4:1, meaning that there are 4 short strands and 1 long strand; to construct pentagon polygons the ratio is 5:1. Additionally, the long strand for each polygon is incrementally increased by two helical turns, ~22 nucleotides (nt). As such, the long strand for the triangle is 66 nt, the square long strand is

88 nt, and the pentagon long strand is 110 nt. Thus, increasing the number of external strands and the length of the internal strand, the angle on the inter-helical ∠AOB increased from 60° to 90° and 108° allowing for 2D formation of corresponding triangle, square, and pentagon polygons (Fig. 2b). However, this approach is limited as stretching ∠AOB to 120° did not result in the formation of a hexagon (results are not shown). The pRNA 3WJ motif has reached a maximum tension, as it appears that stretching of the 3WJ angle past 108° will not result in stable nanoparticles. The measured widths, from one corner to another, were 10.2 nm, while the heights differed as follows: triangle = 9.1 nm, square = 10.2 nm, and pentagon = 12.7 nm (Fig. 2b).

3.4 Sequence Design and Optimization Prior to RNA Synthesis

The final RNA sequences for each polygon were optimized by *mfold* [43] and *nupack* [44] programs to eliminate any stable secondary structures between short strands, between inappropriate regions of long and short strands, and among individual long strands. Each RNA polygon contained identical sequences in each corner corresponding to pRNA 3WJ ∠AOB, which have similar folding energy. The folding energy of the pRNA 3WJ at each corner is believed to be responsible for folding and stability of the polygonal structures. The eight connecting base pairs (bp) and five supporting bp were chosen to be different to prevent nonspecific interactions between short strands. However, the free energy of the duplexes was kept similar, within ±2 kcal/mol ΔG range, to promote fidelity while folding. The resulting sequences and secondary structures of RNA polygons are demonstrated in Fig. 1c with indication of connecting and supporting nucleotides.

3.5 Polygon Assembly

1. Mix RNA strands corresponding to triangle, square, and pentagon (1 μM final concentration) in 1× TMS, and bring final volume to 10 μL with dd H_2O (*see* Table 1).
2. Heat the mixture of RNAs to 80 °C for 5 min and slowly cool down to 4 °C over 1 h. Alternatively, the RNA mixture can be incubated for 37 °C for 30 min to achieve self-assembly.
3. Purify the assembled RNA polygons on native PAGE (6 % acrylamide, in 1× TBM buffer), and run the gel at 80 V for 3–4 h in a cold room.
4. After the gel run is complete, place the gel on TLC plate and excise the RNA band under UV light. Elute RNA from gel slices using 0.5 mL of RNA elution buffer and 10 mM $MgCl_2$.
5. Precipitate RNA polygons with cold ethanol (2.5:1 volume ratio) and 3 M sodium acetate (1:10 volume ratio), rinse twice with cold 80 % ethanol, dry under vacuum, and rehydrate in TMS buffer.
6. Measure RNA concentration and store all samples at −20 °C (please refer to the **Note 4** for troubleshoot).

Table 1
RNA polygon assembly setup

Triangle		Square		Pentagon	
1 µL	10 µM RNA a	1 µL	10 µM RNA a	1 µL	10 µM RNA a
1 µL	10 µM RNA b	1 µL	10 µM RNA b	1 µL	10 µM RNA b
1 µL	10 µM RNA c	1 µL	10 µM RNA c	1 µL	10 µM RNA c
1 µL	10 µM RNA D	1 µL	10 µM RNA d	1 µL	10 µM RNA d
1 µL	10× TMS	1 µL	10 µM RNA E	1 µL	10 µM RNA e
5 µL	ddH_2O	1 µL	10× TMS	1 µL	10 µM RNA F
		4 µL	ddH_2O	1 µL	10× TMS
				3 µL	ddH_2O

3.5.1 Polygons' Thermal Stability Comparison

1. After resuspending PAGE-purified polygons in 1× TMS dilute the stock solutions to 0.5 µM concentration.
2. Follow the Biometra protocol (http://www.biometra.de/) to cast the gel. Use native 6 % polyacrylamide solution in 1× TBM buffer.
3. Run the gel on TGGE using a temperature gradient of 40–80 °C applied at constant 100 V for 1 h.
4. After removing the gel from the TGGE instrument, stain with ethidium bromide solution (*see* **Note 5**), and visualize RNA bands using gel imaging system (e.g., Typhoon FLA 700 GE healthcare (http://www.gelifesciences.com/)).
5. Using ImageJ software (http://imagej.nih.gov/ij/) integrate the intensity of the RNA bands in each well of the gel.
6. Divide the intact nanoparticle intensity (upper most band) by the total intensity of the well to determine nanoparticle formation percentage (example gel is shown in Fig. 3) and plot the data points with temperature on the *x*-axis and percentage of nanoparticle formation on the *y*-axis.
7. Fit the data to a nonlinear fitting curve, taking 50 % nanoparticle formation to be the melting temperature of the polygon.

4 Notes

1. PCR:
   (a) Incorrect size of PCR products might be due to incorrect PCR primer design. Carefully redesign the DNA primers.

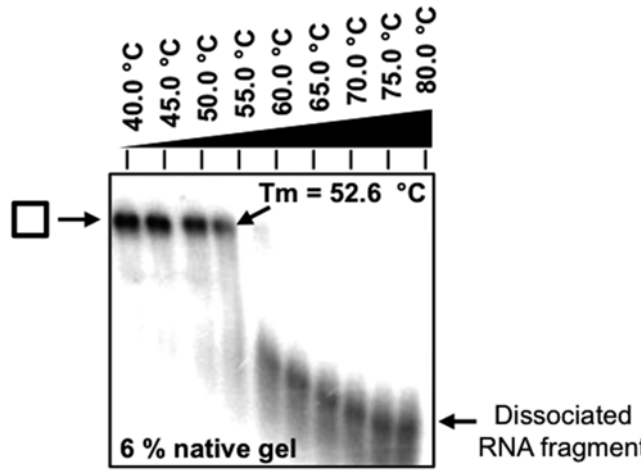

Fig. 3 Representative 6 % TGGE gel of the square RNA polygon melting. The *top bands* represent intact nanoparticle and the downshift is a result of polygon melting

(b) Nonspecific PCR products are usually due to poor PCR condition setup or the fact that primers are incorrectly designed. Optimize PCR conditions and redesign DNA primers.

2. Transcription:
   (a) If product yields are low with a protocol that had already been successfully used for the same template, repeat transcription assay once without any alteration on 20 μL scale. Alternatively, test different enzyme batches or enzymes from alternative suppliers.
   (b) Check that thawed stock solutions, particularly concentrated transcription buffers, do not contain precipitated ingredients.
3. No or low yield of transcription of regular or 2′-F-modified RNA: This is typically due to impure DNA template. Prepare new template DNA; take particular care to effectively remove salts. Check sequence of T7 promoter at the 5′-end of the forward DNA primer.
4. No or low yield of assembled polygons:
   (a) Carefully analyze RNA sequence, run secondary structure folding using Mfold, and thoroughly examine assembly conditions.
5. Determining melting temperature of polygons:
   (a) Ethidium bromide is toxic. Be sure to wear gloves when handling ethidium bromide and only use it in a properly ventilated fume hood.

5 Conclusion

As nanotechnology progresses more challenges are being encountered. One of the most important challenges to overcome is the thermo-stability of RNA nanoparticles. In this chapter we described a simple method to fabricate stable yet functional RNA polygons by stretching the native angle of the RNA three-way junction from phi29 motor pRNA. Polygons that display high yield of formation were achieved via one pot self-assembly of multiple RNA fragments. The key to creating polygons utilizing the same building block is changing the length of the internal RNA strand and increasing numbers of short RNA strands. This induced stretching of the ∠AOB angle of the RNA three-way junction from 60° to 90° and 108°, resulting in self-assembly of elegant RNA triangular, square, and pentagonal nanoparticles. Intermolecular interactions of building blocks within the complex such as kissing loops, receptor loop, or "sticky ends" were avoided by bridging through base pairing between corners of polygons using RNA double helices. Thus, this system is advantageous with increased thermo-stability in the overall construct and yet tunability of the size, and shape of nanoparticles.

Acknowledgements

The work was supported by NIH grants CA151648 and EB003730, and funding to Peixuan Guo's Endowed Chair in Nanobiotechnology position from the William Fairish Endowment Fund. The content is solely the responsibility of the authors and does not necessarily represent the official views of NIH. We would like to acknowledge the core facilities of the Markey Cancer Center at the University of Kentucky.

Conflicts of interest: P.G. is a co-founder of Kylin Therapeutics, Inc.; RNA Nano LLC; and Biomotor and RNA Nanotech Development Co., Ltd.

References

1. Guo P, Zhang C, Chen C, Trottier M, Garver K (1998) Inter-RNA interaction of phage phi29 pRNA to form a hexameric complex for viral DNA transportation. Mol Cell 2:149–155
2. Soni GV, Singer A, Yu Z, Sun Y, McNally B, Meller A (2010) Synchronous optical and electrical detection of biomolecules traversing through solid-state nanopores. Rev Sci Instrum 81:014301
3. Tombelli S, Mascini M (2009) Aptamers as molecular tools for bioanalytical methods. Curr Opin Mol Ther 11:179–188
4. Haes AJ, Van Duyne RP (2002) A nanoscale optical biosensor: sensitivity and selectivity of an approach based on the localized surface plasmon resonance spectroscopy of triangular silver nanoparticles. J Am Chem Soc 124: 10596–10604

5. Afonin KA, Kireeva M, Grabow WW, Kashlev M, Jaeger L, Shapiro BA (2012) Co-transcriptional assembly of chemically modified RNA nanoparticles functionalized with siRNAs. Nano Lett 12:5192–5195
6. Afonin KA, Grabow WW, Walker FM, Bindewald E, Dobrovolskaia MA, Shapiro BA, Jaeger L (2011) Design and self-assembly of siRNA-functionalized RNA nanoparticles for use in automated nanomedicine. Nat Protoc 6:2022–2034
7. Afonin KA, Viard M, Koyfman AY, Martins AN, Kasprzak WK, Panigaj M, Desai R, Santhanam A, Grabow WW, Jaeger L et al (2014) Multifunctional RNA nanoparticles. Nano Lett 14:5662–5671
8. Shu Y, Pi F, Sharma A, Rajabi M, Haque F, Shu D, Leggas M, Evers BM, Guo P (2014) Stable RNA nanoparticles as potential new generation drugs for cancer therapy. Adv Drug Deliv Rev 66C:74–89
9. Shu Y, Haque F, Shu D, Li W, Zhu Z, Kotb M, Lyubchenko Y, Guo P (2013) Fabrication of 14 different RNA nanoparticles for specific tumor targeting without accumulation in normal organs. RNA 19:766–777
10. Shu Y, Shu D, Haque F, Guo P (2013) Fabrication of pRNA nanoparticles to deliver therapeutic RNAs and bioactive compounds into tumor cells. Nat Protoc 8:1635–1659
11. Shu D, Shu Y, Haque F, Abdelmawla S, Guo P (2011) Thermodynamically stable RNA three-way junctions for constructing multifunctional nanoparticles for delivery of therapeutics. Nat Nanotechnol 6:658–667
12. Haque F, Shu D, Shu Y, Shlyakhtenko L, Rychahou P, Evers M, Guo P (2012) Ultrastable synergistic tetravalent RNA nanoparticles for targeting to cancers. Nano Today 7:245–257
13. Qiu M, Khisamutdinov E, Zhao Z, Pan C, Choi J, Leontis N, Guo P (2013) RNA nanotechnology for computer design and *in vivo* computation. Philos Trans R Soc A 371 (2000):201203120
14. Amir Y, Ben-Ishay E, Levner D, Ittah S, Bu-Horowitz A, Bachelet I (2014) Universal computing by DNA origami robots in a living animal. Nat Nanotechnol 9:353–357
15. Reif R, Haque F, Guo P (2013) Fluorogenic RNA nanoparticles for monitoring RNA folding and degradation in real time in living cells. Nucleic Acid Ther 22(6):428–437
16. Shu D, Zhang L, Khisamutdinov E, Guo P (2013) Programmable folding of fusion RNA complex driven by the 3WJ motif of phi29 motor pRNA. Nucleic Acids Res 42:e10
17. Muller MC, Gattermann N, Lahaye T, Deininger MW, Berndt A, Fruehauf S, Neubauer A, Fischer T, Hossfeld DK, Schneller F et al (2003) Dynamics of BCR-ABL mRNA expression in first-line therapy of chronic myelogenous leukemia patients with imatinib or interferon alpha/ara-C. Leukemia 17: 2392–2400
18. Novoa EM, Pavon-Eternod M, Pan T, de Ribas PL (2012) A role for tRNA modifications in genome structure and codon usage. Cell 149: 202–213
19. Motorin Y, Helm M (2010) tRNA stabilization by modified nucleotides. Biochemistry 49:4934–4944
20. Uemura S, Aitken CE, Korlach J, Flusberg BA, Turner SW, Puglisi JD (2010) Real-time tRNA transit on single translating ribosomes at codon resolution. Nature 464:1012–1017
21. Liao J, Yu L, Mei Y, Guarnera M, Shen J, Li R, Liu Z, Jiang F (2010) Small nucleolar RNA signatures as biomarkers for non-small-cell lung cancer. Mol Cancer 9:198
22. Hertel J, Hofacker IL, Stadler PF (2008) SnoReport: computational identification of snoRNAs with unknown targets. Bioinformatics 24:158–164
23. Bachellerie JP, Cavaille J, Huttenhofer A (2002) The expanding snoRNA world. Biochimie 84:775–790
24. Westhof E (2012) Ribozymes, catalytically active RNA molecules. Introduction. Methods Mol Biol 848:1–4
25. Mulhbacher J, St-Pierre P, Lafontaine DA (2010) Therapeutic applications of ribozymes and riboswitches. Curr Opin Pharmacol 10: 551–556
26. Steiner M, Karunatilaka KS, Sigel RK, Rueda D (2008) Single-molecule studies of group II intron ribozymes. Proc Natl Acad Sci U S A 105:13853–13858
27. Breaker RR (2012) Riboswitches and the RNA world. Cold Spring Harb Perspect Biol 4:pii: a003566
28. Wacker A, Buck J, Mathieu D, Richter C, Wohnert J, Schwalbe H (2011) Structure and dynamics of the deoxyguanosine-sensing riboswitch studied by NMR-spectroscopy. Nucleic Acids Res 39:6802–6812
29. Guo P (2010) The emerging field of RNA nanotechnology. Nat Nanotechnol 5:833–842
30. Schroeder A, Goldberg MS, Kastrup C, Wang Y, Jiang S, Joseph BJ, Levins CG, Kannan ST, Langer R, Anderson DG (2012) Remotely activated protein-producing nanoparticles. Nano Lett 12:2685–2689

31. Sternberg SH, Fei J, Prywes N, McGrath KA, Gonzalez RL Jr (2009) Translation factors direct intrinsic ribosome dynamics during translation termination and ribosome recycling. Nat Struct Mol Biol 16:861–868
32. Shoji S, Walker SE, Fredrick K (2009) Ribosomal translocation: one step closer to the molecular mechanism. ACS Chem Biol 4:93–107
33. Schroeder KT, McPhee SA, Ouellet J, Lilley DM (2010) A structural database for k-turn motifs in RNA. RNA 16:1463–1468
34. Ohno H, Kobayashi T, Kabata R, Endo K, Iwasa T, Yoshimura SH, Takeyasu K, Inoue T, Saito H (2011) Synthetic RNA-protein complex shaped like an equilateral triangle. Nat Nanotechnol 6:116–120
35. Guo P, Erickson S, Anderson D (1987) A small viral RNA is required for *in vitro* packaging of bacteriophage phi29 DNA. Science 236:690–694
36. Zhao Z, Khisamutdinov E, Schwartz C, Guo P (2013) Mechanism of one-way traffic of hexameric phi29 DNA packaging motor with four electropositive relaying layers facilitating antiparallel revolution. ACS Nano 7:4082–4092
37. Guo P, Zhao Z, Haak J, Wang S, Wu D, Meng B, Weitao T (2014) Common mechanisms of DNA translocation motors in bacteria and viruses using one-way revolution mechanism without rotation. Biotechnol Adv 32:853–872
38. Binzel DW, Khisamutdinov EF, Guo P (2014) Entropy-driven one-step formation of Phi29 pRNA 3WJ from three RNA fragments. Biochemistry 53:2221–2231
39. Jasinski D, Khisamutdinov EF, Lyubchenko YL, Guo P (2014) Physicochemically tunable poly-functionalized RNA square architecture with fluorogenic and ribozymatic properties. ACS Nano 8:7620–7629
40. Khisamutdinov EF, Jasinski DL, Guo P (2014) RNA as a boiling-resistant anionic polymer material to build robust structures with defined shape and stoichiometry. ACS Nano 8:4771–4781
41. Khisamutdinov E, Li H, Jasinski D, Chen J, Fu J, Guo P (2014) Enhancing immunomodulation on innate immunity by shape transition among RNA triangle, square, and pentagon nanovehicles. Nucleic Acids Res 42:9996–10004
42. Lescoute A, Westhof E (2006) Topology of three-way junctions in folded RNAs. RNA 12:83–93
43. Zuker M (2003) Mfold web server for nucleic acid folding and hybridization prediction. Nucleic Acids Res 31:3406–3415
44. Zadeh JN, Steenberg CD, Bois JS, Wolfe BR, Pierce MB, Khan AR, Dirks RM, Pierce NA (2011) NUPACK: Analysis and design of nucleic acid systems. J Comput Chem 32: 170–173